This article has been accepted by the IFAC journal of *Control Engineering Practice*

Power System Observability and Dynamic State Estimation for Stability Monitoring Using Synchrophasor Measurements ⋆

Kai Sun * **Junjian Qi** ** **Wei Kang** ***

* *Department of EECS, University of Tennessee, Knoxville, TN 37996 USA (e-mail: kaisun@utk.edu)*
** *Energy Systems Division, Argonne National Laboratory, Argonne, IL 60439 USA (e-mail: jqi@anl.gov)*
*** *Department of Applied Mathematics, Naval Postgraduate School, Monterey, CA 93943 USA (e-mail: wkang@nps.edu)*

Abstract: Growing penetration of intermittent resources such as renewable generations increases the risk of instability in a power grid. This paper introduces the concept of observability and its computational algorithms for a power grid monitored by the wide-area measurement system (WAMS) based on synchrophasors, e.g. phasor measurement units (PMUs). The goal is to estimate real-time states of generators, especially for potentially unstable trajectories, the information that is critical for the detection of rotor angle instability of the grid. The paper studies the number and siting of synchrophasors in a power grid so that the state of the system can be accurately estimated in the presence of instability. An unscented Kalman filter (UKF) is adopted as a tool to estimate the dynamic states that are not directly measured by synchrophasors. The theory and its computational algorithms are illustrated in detail by using a 9-bus 3-generator power system model and then tested on a 140-bus 48-generator Northeast Power Coordinating Council power grid model. Case studies on those two systems demonstrate the performance of the proposed approach using a limited number of synchrophasors for dynamic state estimation for stability assessment and its robustness against moderate inaccuracies in model parameters.

Keywords: Observability; Dynamic State Estimation; Synchrophasor; PMUs; Rotor Angle Stability; Unscented Kalman Filter.

1. INTRODUCTION

The penetration of a large number of intermittent power generations using renewable energy brings increasing uncertainties to daily operations of interconnected power grids. Early indicating wide-area stability problems is crucially important for control centers to prevent cascading power outages and blackouts (Dobson [2001], Qi [2013], Qi, Sun, Mei [2015]). In the US and many other countries, synchrophasors, e.g. Phasor Measurement Units (PMUs), are being installed and networked onto transmission systems to provide high-resolution wide-area measurements synchronized using real-time GPS signals. Electricity utilities are building PMU networks to collect data from dispersed PMUs and then send the data to online stability applications at control centers. As of today there are still large technical gaps in applying PMU data effectively for real-time stability analysis and for the control of power grids. Most existing PMU applications are based on direct visualization of PMU data for operators to monitor the grid, which, however, cannot provide in-depth information about the dynamic behavior of the whole grid under disturbances, e.g. contingencies, load changes and unpredictable variations with renewable generations.

In fact, the data in time series collected from networked PMUs makes it possible to reliably predict the dynamic behavior of the entire grid. Thus, the observability based on data from networked PMUs and methods of real-time state estimation of the dynamic grid need to be studied (Kang [2013]). The goal of this paper is to develop and validate the fundamental theory and the methodology for designing efficient PMU networks by maximizing the observability of potential instabilities and unmeasured states. In addition, a unscented Kalman filter (UKF) based data fusion algorithm is also developed. Some fundamental questions on designing a PMU network are such as how to evaluate networked PMUs in terms of the observability to the presence of instability, and how to develop computationally efficient algorithms for estimating state variables not directly measured by PMUs.

While the theory and algorithms for the filtering and optimal sensor design have been developed for many years, some recent results in Kang-Xu [2009a,b] can be used to quantitatively measure observability for large-scale nonlinear systems. Methodologies of optimal sensor placement based on observability Gramian have been developed for weather prediction (Kang-Xu [2012]) and chemical engineering (Singh [2005, 2006]). In power systems, most of research on PMU placement is for static state estimation and, hence, is mainly based on the topological observability criterion and focuses on the binary connectivity graph (Baldwin [1993]). Under this framework, many optimization approaches have been proposed, e.g. mixed integer programming (Xu [2004], Gou [2008]), binary search (Chakrabarti [2008]) and genetic algorithms (Milosevic [2003], Aminifar [2009]).

⋆ This work was supported in part by the University of Tennessee, Knoxville, the CURENT Engineering Research Center, and AFOSR.

In this paper, we extend existing results on observability and dynamic state estimation for nonlinear dynamic systems to explore and analyze the observability of power grids and to address some of the aforementioned issues on PMU network design. In Section 2, we first introduce the concept of observability and its computational algorithm. This concept is fundamental to the evaluation of PMU networks. It is utilized to determine the number and siting of PMUs so that the state of the system can be accurately estimated in the presence of instability. Then, an UKF is introduced as a tool to estimate the states that are not directly measured by PMUs. In Sections 3 and 4, we illustrate the methodology developed in detail using a 9-bus 3-generator power system model. In Section 5, we test its performance on a 140-bus 48-generator power system, i.e. a reduced model of the Northeast Power Coordinating Council (NPCC) power grid in North America.

2. OBSERVABILITY AND UKF

This section introduces the concept of unobservability index and an UKF based state estimation method.

2.1 Observability

In Kang-Xu [2009a,b], a quantitative measure of partial observability is defined for general dynamical systems. For power systems, we adopt a simplified version of that definition. Consider any system defined by ordinary differential equations (1), where $x \in I\!R^n$ is the state variable and $y(t) \in I\!R^m$ is the output given by sensor measurement.

$$\begin{aligned} \frac{dx(t)}{dt} &= f(t, x(t)), \\ y(t) &= h(x(t)). \end{aligned} \tag{1}$$

In this section, we define the observability with initial condition $x(0)$, which uniquely determines the trajectory of a system. The definition can be easily modified to define the observability for $x(t_0)$ with any given time $t = t_0$. Suppose x and y lie in normed spaces with norms denoted by $||x||$ and $||y||_Y$.

Definition 1. Given $\rho > 0$ and a nominal trajectory $x(t)$ of (1). Let

$$\epsilon^N = \inf ||h(\hat{x}(t)) - h(x(t))||_Y \tag{2}$$

where $\hat{x}(t)$ satisfies

$$\frac{d\hat{x}}{dt} = f(t, \hat{x}) \tag{3}$$

Let $||\hat{x}(0) - x(0)|| = \rho$, and define ρ/ϵ as the unobservability index (UI) of $x(0)$.

Remark. As a quantitative measure of observability, the ratio ρ/ϵ can be interpreted as follows: if the maximum error of the measured output, or sensor error, is ϵ, then the worst estimation error of $x(0)$ is ρ. Therefore, a small value of ρ/ϵ implies strong observability of $x(0)$. For linear systems with a L^2-norm, it can be proved that the reciprocal of the unobservability index is the square root of the smallest eigenvalue of the observability gramian.

Definition 1 can be numerically implemented for nonlinear systems. In this paper, two algorithms are used to compute the UI, namely the empirical gramian method and the method of pseudospectral dynamical optimization. Empirical gramian is a method of first order approximation for the UI. The idea is to approximate the UI using the smallest eigenvalue of a gramian matrix (Krener [2009], Kang-Xu [2009a,b]). Due to its simplicity, this method is used for most cases in this paper. However, for the problem of robust observability, that method is not accurate enough. Alternatively, we use a more sophisticated algorithm based on pseudospectral method (Gong [2006]).

2.2 Unscented Kalman Filter (UKF)

For systems with strong or reasonable observability, filters can be used as virtual sensors to estimate the variables that are not directly measured. Kalman filter was developed originally for linear systems. Modified Kalman filters are widely used for nonlinear systems. Extended Kalman filter has been utilized in power system state estimation for stability control purposes (e.g. Baechle [2014]). However, it requires the linearization of system models, which may not be easily available during real-time operations for large-scale systems like power grids. This paper adopts UKF, which does not require online computation of system linearization. UKF is used as virtual sensors to estimate both state variables and uncertain parameters. It is also used as a tool to verify the observability computed using different methods. Consider a nonlinear system

$$\begin{aligned} x_n &= f(x_{n-1}, w_{n-1}) \\ y_n &= h(x_{n-1}, v_{n-1}) \end{aligned} \tag{4}$$

where x, y, w, and v represent the state, measurement, process noise, and measurement noise, respectively. The UKF is "founded on the intuition that it is easier to approximate a probability distribution than it is to approximate an arbitrary nonlinear function or transformation" Julier-Uhlmann [2004]. The algorithm of an UKF is outlined as follows. Details can be found in Julier-Uhlmann [2004].

- Based on the previous-step estimation of the state, $\hat{x}_{n-1}$, and the covariance matrix, $\hat{P}^{xx}_{n-1}$, calculate a set of sigma points as

$$\sigma^i = \hat{x}_{n-1} \pm \sqrt{N_x \hat{P}^{xx}_{n-1}},\ i = 1, 2, \ldots, N_x. \tag{5}$$

- Propagate all the sigma points through the nonlinear dynamic and the output equations,

$$z^i = f(\sigma^i, 0),\ g^i = h(\sigma^i, 0),\ i = 1, 2, \ldots, N_x. \tag{6}$$

- Calculate predicted means of the state and output,

$$\tilde{x}_n = \frac{1}{2N_x} \sum_{i=1}^{2N_x} z^i,\ \tilde{y}_n = \frac{1}{2N_x} \sum_{i=1}^{2N_x} g^i. \tag{7}$$

- Predictions of the covariance matrices are given by

$$\begin{aligned} \tilde{P}^{xx}_n &= \frac{1}{2N_x} \sum_{i=1}^{2N_x} (z^i - \tilde{x}_n)(z^i - \tilde{x}_n)^T \\ \tilde{P}^{yy}_n &= \frac{1}{2N_x} \sum_{i=1}^{2N_x} (g^i - \tilde{y}_n)(g^i - \tilde{y}_n)^T \\ \tilde{P}^{xy}_n &= \frac{1}{2N_x} \sum_{i=1}^{2N_x} (z^i - \tilde{x}_n)(g^i - \tilde{y}_n)^T. \end{aligned} \tag{8}$$

Once the predictions of $\tilde{x}_n$, $\tilde{P}^{xx}_n$, $\tilde{P}^{yy}_n$, and $\tilde{P}^{xy}_n$ are available, the update is given by

$$\hat{x}_n = \tilde{x}_n + K(y_n - \tilde{y}_n) \tag{9}$$

where $K = \tilde{P}^{xy}_n [\tilde{P}^{yy}_n]^{-1}, \hat{P}^{xx}_n = \tilde{P}^{xx}_n - K \tilde{P}^{xy}_n K^T$.

3. OBSERVABILITY ANALYSIS ON THE BOUNDARY OF THE DOMAIN OF ATTRACTION

To provide adequate information for stability monitoring, it is important to verify that the system is reasonably observable both before and at the time of loss of instability.

Given a set of PMUs, the UI can be computed to determine if the system is adequately observable around the boundary of the domain of attraction (DOA) about system states. Theoretically speaking, the UI should be evaluated for sampling points of enough density on the boundary of the DOA since the system may pass any of those points to lose stability. However, the DOA usually exists in the high dimensional state space. Discretizations of geometric surfaces in high dimensions suffer the curse of dimensionality, i.e. the number of sampling points increases at an exponential rate so that it quickly exceeds a computer's capability. Therefore, reducing the dimension of the system model may significantly simplify the problem. For the 9-bus system, we directly reduce dimensions of the state equations for visualization protected onto a 3D state space. Later, in Section 5 for the 140-bus NPCC system, we investigate those sampling points on the boundary that are related to only credible "N-1" contingencies (i.e. loss of a single component) based on standard power system protection settings.

3.1 Identification of the boundary of the DOA

First, consider the following n-bus power system whose generators are represented by the $2nd$-order classic model,

$$\begin{aligned} \dot{\delta}_i &= \omega_i - \omega_R, \\ \dot{\omega}_i &= \frac{\omega_R}{2H_i}\big[(T_{mi} - T_{ei} - D_i\frac{\omega_i - \omega_R}{\omega_R}\big] \end{aligned} \tag{10}$$

where i is the generator serial number, rotor angle δ_i and rotor speed ω_i are state variables, T_{mi} is mechanical torque, T_{ei} is electric air-gap torque, ω_R is the rated value of angular frequency, H_i is the inertia constant, and D_i is the damping factor, and

$$T_{ei} = E_i^2 G_{ii} + \sum_{j=1, j\neq i}^{n} E_i E_j Y_{ij} \cos(\theta_{ij} - \delta_i + \delta_j). \tag{11}$$

Proposition 1 Sun [2014]. Suppose $(\delta_i(t), \omega_i(t))$, $i = 1, 2, \cdots, n$, is a solution of (10). Let δ_0 and ω_0 be constant numbers.

(a) $(\bar{\delta}_i(t), \bar{\omega}_i(t))$, $i = 1, 2, \cdots, n$, is a solution of (10), where

$$\bar{\delta}_i(t) = \delta_i(t) + \delta_0, \;\; \bar{\omega}_i(t) = \omega_i(t). \tag{12}$$

(b) If $D_i = 0$, then $(\bar{\delta}_i(t), \bar{\omega}_i(t))$, $i = 1, 2, \cdots, n$, is a solution of (10), where

$$\bar{\delta}_i(t) = \delta_i(t) + \omega_0 t, \;\; \bar{\omega}_i(t) = \omega_i(t) + \omega_0. \tag{13}$$

The 9-bus system model from Anderson-Fouad [1994], as shown in Fig 1, is used to illustrate the evaluation of the proposed UI. Parameters are: $\omega_R = 2\pi \cdot 60$ Hz, $D_1 = D_2 = D_3 = 0$, H_1=47.28 s, H_2=12.8 s, H_3=6.02 s, E_1=1.0566 p.u., E_2=1.0502 p.u., E_3=1.0170 p.u., Power Base = 100 MVA, T_{m1}=0.716 p.u., T_{m2}=1.63 p.u., T_{m3}=0.85 p.u..

The reduced Y matrix is

$$\begin{bmatrix} 0.8455 - j2.9883 & 0.2871 + j1.5129 & 0.2096 + j1.2256 \\ 0.2871 + j1.5129 & 0.4200 - j2.7239 & 0.2133 + j1.0879 \\ 0.2096 + j1.2256 & 0.2133 + j1.0879 & 0.2770 - j2.3681 \end{bmatrix}. \tag{14}$$

The system has an equilibrium

$$\begin{aligned} &[\,\delta_1 \;\; \delta_2 \;\; \delta_3\,]^T = [\,2.2717^\circ \;\; 19.7315^\circ \;\; 13.1752^\circ\,]^T \\ &\omega_i = \omega_R, \;\; i = 1, 2, 3. \end{aligned} \tag{15}$$

Around any equilibrium of nonlinear systems there is a DOA. The trajectory starting from any point in it converges to the equilibrium. However, there is no general way of computing the DOA. Although Zubov's equation defines its boundary, this equation is extremely difficult to solve, numerically or analytically, if not impossible. On the other hand, practical criteria based on experimentations can be used to approximate a DOA. It is desired that

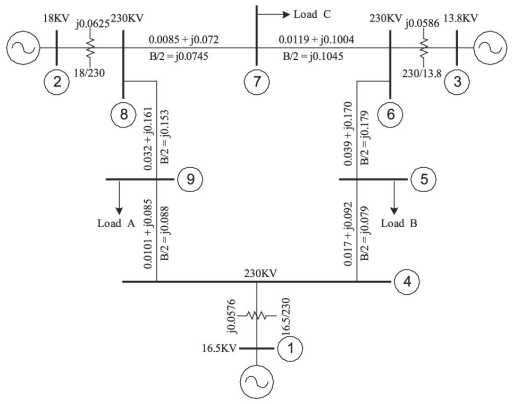

Fig. 1. A 9-bus 3-generator system and parameters

the data collected by PMUs make the system strongly observable at the boundary of the DOA, which implies that all state information can be reliably estimated for analysis and control before a trajectory becomes unstable.

In the following, we find a layer outside the boundary of the DOA, starting from which all trajectories lost its stability. Adequate simulations on the 9-bus system indicate that stability is lost quickly after at least one angle relative to a preselected reference angle becomes $> 650^\circ$. Therefore, this practical criterion is used to compute an envelop outside the DOA: *all initial angles so that at least one relative angle is between* 650° *and* 750° *at* $t = 5s$.

Using Proposition 1, we can reduce the dimension in the description of the DOA by 2. For example, the state space of a 9-bus model has six state variables, (δ_i, ω_i), $i = 1, 2, 3$. The boundary of the DOA is a $5D$ surface, which cannot be visualized using $3D$ graphs. However, we can focus on trajectories $(\delta_i(t), \omega_i(t))$ in which $\delta_3(0)$ and $\omega_3(0)$ have these fixed values, i.e. from the equilibrium (15),

$$\delta_3(0) = 13.1752^\circ, \;\; \omega_3(0) = \omega_R. \tag{16}$$

More specifically, we find the envelope of the DOA in the $4D$ subspace $[\,\delta_1(0) \;\; \delta_2(0) \;\; \omega_1(0) \;\; \omega_2(0)\,]$ with fixed initial values for δ_3 and ω_3. Any initial values in the envelope of the DOA in the original $6D$ space can be transferred, using (12)-(13), into a trajectory with initial state satisfying (16). Therefore, every trajectory in the $6D$ space is equivalent to a trajectory with an initial state in a reduced $4D$ subspace. For the purpose of finding the DOA, this implies that we only compute an envelope in the $\delta_1\delta_2\omega_1\omega_2$-subspace.

Following Proposition 1, we consider a "slice" or section of the DOA in the subspace in which δ_3 and ω_3 are fixed. The DOA in the full state space can be achieved by the transformation (12)-(13). This method of dimension reduction is especially efficient for $5D$ or $6D$ problems because the domain with a reduced dimension can be visualized by using $3D$ graphics. Using the 9-bus model as an example, an envelope is a $5D$ surface in the $6D$ state space. The envelope with a reduced dimension is a $3D$ surface in a $4D$ space, i.e. the $\delta_1\delta_2\omega_1\omega_2$-subspace. We cannot visualize its geometry in a $4D$ space, but can visualize its sections in a sequence of $3D$ subspaces. As an example, we assign a sequence of values to ω_2,

$$\begin{aligned} &\omega_2 = \omega_R + \Delta\omega \\ &\Delta\omega = -1, -0.5, 0, 0.5, 1 \;\; \text{Hz}. \end{aligned} \tag{17}$$

For each fixed value of ω_2, compute an envelope for the DOA in $\delta_1\delta_2\omega_1$-space. This section of envelope is a $2D$ surface. The following algorithm can search for sampling

points in the envelope. The grid points for ω_1 is a sequence in the interval $[\omega_R - 2, \omega_R + 2]$ (Hz):

$$\omega_1^k = \omega_R - 2 + 0.1k \text{ Hz}, \quad k = 0, 1, 2, \cdots, 21. \tag{18}$$

For each value of ω_1, a 360° search around the equilibrium (15) is carried out numerically for a sequence of directions,

$$v_j = [\cos(\theta_j) \ \sin(\theta_j)]^, \ \theta_j = 3^\circ \times j, \ j = 1, 2, \cdots, 120.$$

For each ω_1^k in (18), one point in the envelope of the DOA is found in the direction of v_j,

$$[\,2.2717^\circ \ \ 19.7315^\circ\,] + r \times v_j \tag{19}$$

in which the radius r is determined as follows.

(1) Find $r_{\min}$ and $r_{\max}$ so that the system is stable and unstable respectively with $r = r_{\min}$ and $r_{\max}$ in initial condition (19).
(2) Let $r = (r_{\max} + r_{\min})/2$. Solve ODE (1) using (19).
(3) Check $\Delta = \max\{|\delta_2(T) - \delta_1(T)|, |\delta_3(T) - \delta_1(T)|\}$, where $T = 5$. If $\Delta > 750^\circ$, then $r_{\max} = r$ and go to step (2); if $\Delta < 650^\circ$, then $r_{\min} = r$ and go to step (2); if $650^\circ \le \Delta \le 750^\circ$, stop, and the point (19) is in the envelope of the DOA.

For each value of ω_2 and ω_1, this algorithm is applied to 120 different directions, v_j. In each $3D$ section of the envelope with a fixed ω_2, a total of $22 \times 120 = 2,640$ sampling points are found in the envelope. We computed five such sections using values from (17) so that the overall envelope of the DOA is approximated by $13,200$ sampling points. 2 of the 5 sections of the envelope of the DOA are illustrated in Fig. 2. From the figures, the boundary is not smooth. This is in fact possible for nonlinear dynamical systems in which the boundary consists of trajectories as well as equilibrium points. However, details about the system behavior around the nonsmooth boundary points require further investigation that is out the scope of this paper. Trajectories starting from this surface diverge after about $t = 5$s. A typical trajectory is shown in Fig. 3.

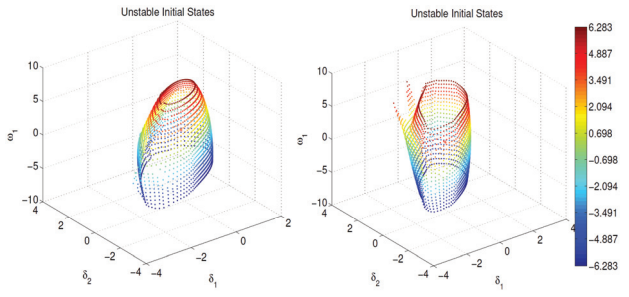

Fig. 2. Envelopes of the DOA in $\delta_1\delta_2\omega_1$-space with $\Delta\omega_2 = -1$ and 0 Hz

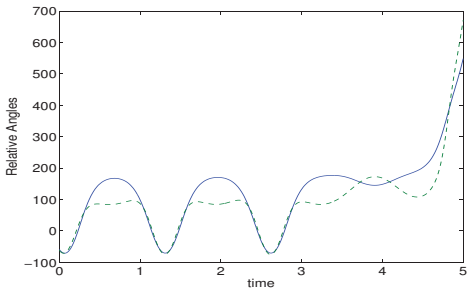

Fig. 3. Relative angles of an unstable trajectory. Solid line: $\delta_2 - \delta_2$; dashed line: $\delta_3 - \delta_1$

3.2 Observability and nonlinear estimation

For the purpose of detecting instability, the PMUs should be installed so that trajectories near the DOA should be observable. In the following, the quantitative observability in Definition 1 is applied to all points in the envelope of the DOA. Assume that a PMU is installed at Generator 1 and δ_1 and ω_1 can be directly measured. Then the output function is $y = [\,\delta_1 \ \omega_1\,]^T$. We assume that PMU collects data at its typical data rate 30 Hz. The norms in Definition 1 are defined as

$$||y(t)||_Y^2 = \frac{1}{30}\sum_{j=1}^{30} [\,\delta_1 \ \omega_1\,] W_1^2 \begin{bmatrix}\delta_1\\ \omega_1\end{bmatrix} \tag{20}$$

where W_1 is the weight matrix

$$W_1 = \begin{bmatrix} 1/R_\delta & 0 \\ 0 & 1/R_\omega \end{bmatrix}, \quad \begin{matrix} R_\delta = 0.01 \cdot \frac{\pi}{180} \\ R_\omega = 2\pi \cdot 5 \cdot 10^{-3}. \end{matrix} \tag{21}$$

This weight matrix is chosen based on the assumption that the error of δ is bounded by 0.01° and the error for ω is bounded by 5×10^{-3} Hz. The metric for state variables is

$$||x||^2 = x^T W_2^2 x \tag{22}$$

where $x = [\,\delta_1 \ \delta_2 \ \delta_3 \ \omega_1 \ \omega_2 \ \omega_3\,]^T$ and the weight matrix, W_2, is defined as follows,

$$W_2 = \begin{bmatrix} \frac{50}{R_\delta} I_3 & 0 \\ 0 & \frac{50}{R_\omega} I_3 \end{bmatrix}, \quad I_3 \text{ is an identity matrix.} \tag{23}$$

This weight matrix implies that $50 \times 0.01 = 0.5^\circ$ and $50 \times 5 \times 10^{-3} = 0.25$ Hz are considered good accuracy in estimation. The UI is a number describing the smallest input-to-output gain from the initial state to the variables measured by sensors. It means that the worst estimation error of the state variable is UI times the sensor error, in their corresponding metrics. For the purpose of instability analysis, the goal is to have reasonable estimate that can tell the trends of the state variables. For this purpose, trajectories with 0≤UI<1 are strongly observable; 1≤UI≤30 are reasonably observable; UI>30 are weakly observable, sometimes unobservable.

The algorithm of computing the first order approximation of UI using empirical gramian is outlined as follows. It is inspired by the work of Krener [2009]. We use weighted norms based on the noise covariance. Let $\rho > 0$ be a small number that represents the error tolerance in estimation. Let $x \in I\!R^n$ represent the state variable consisting of δ_i and ω_i. Let $\{X_1, X_2, \cdots, X_n\}$ be a basis of $I\!R^n$. In the case of the 9-bus model, $n = 6$. Given any initial condition x_0 on the envelope of DOA, we solve the ODE model of the system to compute

$$\begin{aligned} &\Delta_i(t) = \frac{1}{2\rho}\left(y(t; x_0 + \rho X_i) - y(t; x_0 - \rho X_i)\right) \\ &G_{ij} = <\Delta_i, \Delta_j>_{W_1}, \quad S_{ij} = <X_i, X_j>_{W_2}. \end{aligned} \tag{24}$$

For the 9-bus model,

$$\begin{aligned} <\Delta_i, \Delta_j>_{W_1} &= \frac{1}{30}\sum_{k=1}^{30} \Delta_i(t_k)^T W_1 \Delta_j(t_k) \\ <X_i, X_j>_{W_2} &= X_i^T W_2 X_j. \end{aligned} \tag{25}$$

Let $\sigma_{\min}$ be the smallest eigenvalue of G relative to S, i.e.

$$G\xi = \sigma_{\min} S\xi. \tag{26}$$

For some $\xi \neq 0$, the UI is approximated by $\dfrac{1}{\sqrt{\sigma_{\min}}}$.

Once again, the empirical gramian algorithm is used in the computation. We focus on the observability in the time

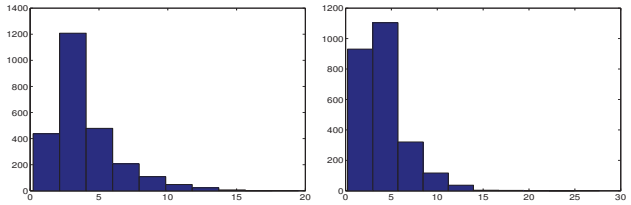

(a) $\Delta\omega_2 = -1$ and -0.5 Hz

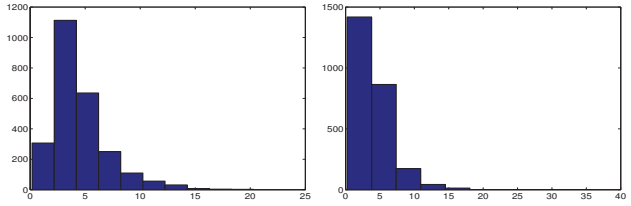

(b)$\Delta\omega_2 = 0$ and 0.5 Hz

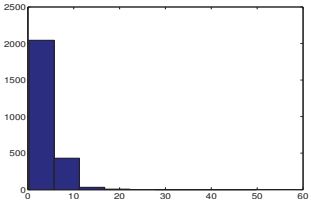

(c)$\Delta\omega_2 = 1$ Hz

Fig. 4. The histograms of the unobservability index

interval $[4, 5]$ (s), i.e. the last second before the trajectory loses its stability. Each value of $\Delta\omega_2 = -1, -0.5, 0, 0.5, 1$ Hz determines a 3D section of the envelope as shown in Fig. 2. For each section, a histogram about the UI is drawn as shown in Fig. 4. For all trajectories initiated from these sections, we compute their UIs. The histograms show the value of the UI vs. the number of initial states in the envelope. Except for a few special cases, all trajectories are either strongly or reasonably observable (UI<30). The worst observability is over 40 when $\Delta\omega_2 = 0.5$ and 1 Hz.

UKF is applied to observable trajectories. As expected, for almost all initial states in the envelope the estimates for both the angles and the angular velocities track the true value closely when the system loses stability. However, for trajectories with high UIs the estimator is not always reliable. In some cases, UKF works fine, but in some other cases it fails to track the true trajectory. For instance, we applied UKF to the trajectory with the worst observability, UI=63.95. The result is fine as shown in Figs. 5 and 6. Although the errors are not small, the estimates are able to follow the trend of the true trajectory, an important feature used in power system stability analysis.

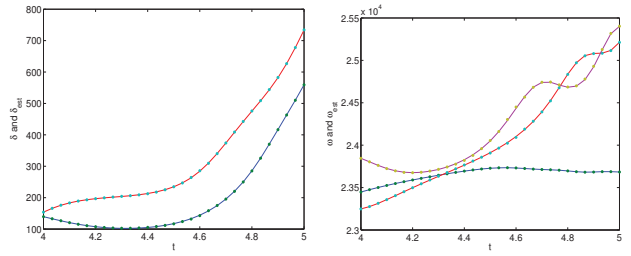

Fig. 5. UKF estimates (star) with UI= 63.95

If PMU is installed at Generator 2 (the least observable trajectory has UI=40.22), UKF cannot track the trends of the trajectory when it goes unstable (Figs. 7 and 8).

For the same trajectories, the observability is changed if the PMU is installed at a different generator. We computed

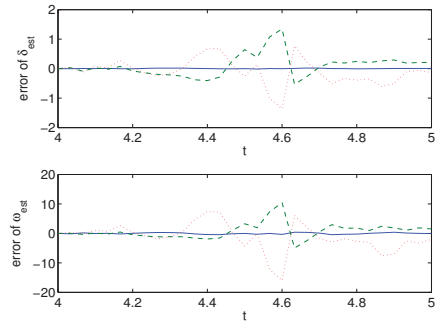

Fig. 6. UKF estimation errors with UI = 63.9457

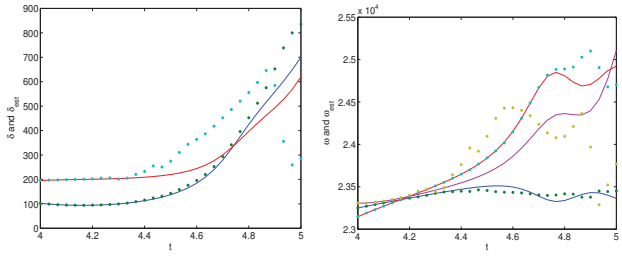

Fig. 7. UKF estimates (star) with UI= 40.22

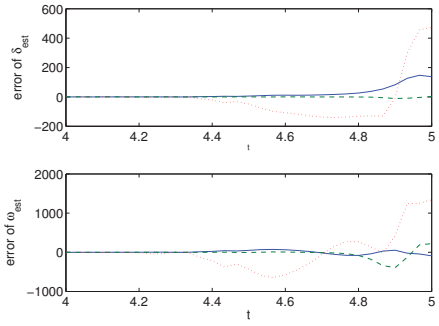

Fig. 8. UKF estimation errors with UI= 40.22

the UI for all three generators. The results are similar to what is shown above, i.e. almost all trajectories are reasonably observable. Among all 13,200 trajectories from the envelope of the DOA with a PMU located in any of the three generators, there are only three trajectories with weak observability, UI> 30. The case studies on the 9-bus system show that, even if the system is mostly observable, it cannot be concluded that the overall system is always observable. There could be very small neighborhoods in which observability drops significantly.

4. OBSERVABILITY AND ESTIMATION IN THE PRESENCE OF SYSTEM UNCERTAINTIES

System instabilities can be triggered by two different reasons, an initial state outside the DOA or a change of system parameters. The former is studied in the previous section. In this section, we first study the robustness of the observability in the presence of unknown parameter changes, and then introduce an adaptive nonlinear estimation method to provide accurate state estimate. In addition, some unknown parameters can also be estimated using sensor information.

4.1 Robustness of observability

Let δ_i^e and ω_i^e, $i = 1, 2, 3$, be the equilibrium point (15) of the system in (1) with a reduced Y matrix (14). At

time $t = 0$, we assume that the system's admittance matrix is changed due to, e.g., a contingency, i.e. $\bar{Y} = Y + \Delta Y$, which is not known to the operator. If the estimation is still based on the original Y matrix, how robustness is the observability? To quantitatively measure the robustness of observability, we use the remainders of trajectories, an approach from Kang [2011]. Suppose the PMU measures $\delta_1(t)$ and $\omega_1(t)$. Let $\delta_i(t)$ and $\omega_i(t)$, $i = 1, 2, 3$, be a trajectory with the new $\bar{Y}$ matrix starting from the equilibrium (15). Suppose $\delta_i^*(t)$ and $\omega_i^*(t)$ be the best estimate of $\delta_i(t)$ and $\omega_i(t)$ using the original Y matrix,

$$\begin{array}{l} \min || \left[\tilde{\delta}_1(t) - \delta_1(t) \;\; \tilde{\omega}_1(t) - \omega_1(t) \right] ||_{W_1} \\ \tilde{\delta}_i(t) \text{ and } \tilde{\omega}_i(t) \text{ satisfy (10)-(14)} \end{array} \quad (27)$$

where W_1 is defined in (21). Let $\delta_i^r(t) = \delta_i(t) - \delta_i^*(t)$ and $\omega_i^r(t) = \omega_i(t) - \omega_i^*(t)$ be the remainder, then

$$\delta_i(t) = \delta_i^*(t) + \delta_i^r(t), \; \omega_i(t) = \omega_i^*(t) + \omega_i^r(t). \quad (28)$$

According to (27), $\delta_i^*(t)$ and $\omega_i^*(t)$ are the best estimates of $\delta_i(t)$ and $\omega_i(t)$ using the matrix Y and the sensor information. The estimation error is the remainder, $\delta_i^r(t)$ and $\omega_i^r(t)$. This error is not directly caused by the output noise, i.e. this error cannot be reduced no matter how accurate the output is measured. Therefore, the remainder is a measure of the robustness of observability. If the remainder is small, it implies that a nonlinear estimator is able to accurately estimate the state variables in the presence of small unknown parameter change.

To compute the remainder and the best estimate, we must solve (27). It is a problem of nonlinear dynamic optimization. An analytic solution does not exist. Here, computational dynamic optimization is applied. To solve (27), this paper adopts a pseudo-spectral method of computational optimal control based on Legendre-Gauss-Lobatto quadrature nodes, which has been actively studied in the literature (see, for instance, references Fahroo-Ross [1998], Gong [2006]). It consists of two parts, a discretization method and a nonlinear programming (NLP) solver. The discretization is based on a set of nodes in the time interval, $t_0 < t_1 < \cdots < t_N$. The nodes used in a pseudo-spectral method are determined based upon orthogonal polynomials, for instance the Legendre-Gauss-Lobatto nodes that consists of $\{-1, 1\}$ and all zeros of the derivative of a Legendre polynomial. A state trajectory $x(t)$ is approximated by N vectors $\{\bar{x}^{Nj}\}_{j=0}^N$ at the nodes, i.e.

$$\bar{x}^{Nj} \approx x(t_j), \;\; \bar{u}^{Nj} \approx u(t_j), \;\; j = 0, 1, \cdots, N \quad (29)$$

The differential equations in the power system model are transformed into a set of nonlinear algebraic equations of $\{\bar{x}^{Nj}\}_{j=0}^N$. As a result, the optimization problem (27) is approximated by a NLP, which is a finite dimensional optimization constrained by algebraic equations. Then an NLP numerical solver using sequential quadratic programming is applied to find an estimated solution of (27) .

As an example, we compute the remainder for a ΔY in which all entries are zero except $\Delta Y_{12} = \Delta Y_{21} = \gamma Y_{12}$ and $\gamma = -0.01$, i.e. the entries Y_{12} and Y_{21} in Y are reduced by 1% in magnitude. For the time interval $[0, 1]$, the remainder is shown in Fig. 9. The magnitude of the remainders depends on the length of the time interval and are found to increase with the final time T. Use the final-time error as a metric for the remainder, i.e. $|| \left[\delta_1^r(T) \;\; \delta_2^r(T) \;\; \delta_3^r(T) \right] ||$ and $|| \left[\omega_1^r(T) \;\; \omega_2^r(T) \;\; \omega_3^r(T) \right] ||$, the results for $T = 1, 2, 3, 4, 5$ (s) is also shown in Fig. 9, where "$*$" represents the norm of angles in "deg" and 'o' represents the norm of angular velocities in "deg/s", which respectively increase linearly and at a higher order. The result implies that the UI is "unstable" in the sense that the remainder's magnitude, i.e. the error of the best estimate, increases with time. Therefore, the observability decreases as time goes on, and hence is not robust to the variation of system parameters.

Table 1. UI with parameter variations

20% change	UI	20% change	UI
Y_{12}	0.8572	Y_{12} and Y_{13}	1.2585
Y_{13}	1.7593	Y_{12} and Y_{23}	0.7026
Y_{23}	0.8055	Y_{13} and Y_{23}	1.3826

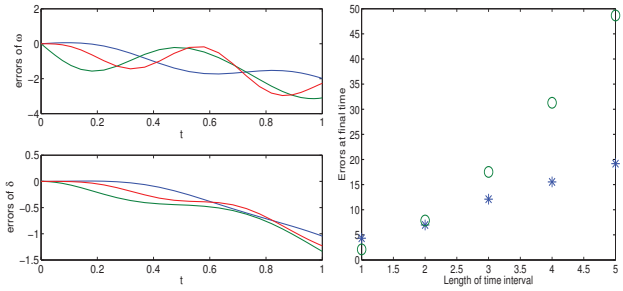

Fig. 9. The remainders for the first 1 s (left) and for $T = 1, 2, 3, 4, 5$ (right)

4.2 The observability of inaccurate parameters and adaptive estimation

Given the robustness study, it is important to make a state estimator adaptive to an unknown parameter change. In fact, we can compute the observability of both the state variables and the parameters in the system model. More specifically, suppose the inaccurate parameter is the magnitude of Y_{12}, then $\bar{Y}_{12} = \gamma Y_{12}$. If $\gamma = 1$, the nominal value of Y is the same as the true value. If $\gamma \neq 1$, the parameter in the system is varied. In this case, we want to estimate the change and then adaptively adjust the estimates. For this purpose, we define the observability of both state variables ω_i and δ_i and r using Definition 1 and this norm

$$||x||^2 = x^T W_2 x + W_3 r^2 \quad (30)$$

where W_2 is from (23) and $W_3 = 1/0.05$. The nominal value, γ, in the simulations is 0.8, i.e. we assume a 20% parameter variation that is unknown. Observability of the parameter variation as well as the state variables is computed and listed in Table 1. From the table we can conclude that parameter variations are observable. For instance, if Y_{12} is varied by 20%, the unobservability index is 0.9853, which implies strong observability. If two parameters are unexpectedly changed by 20%, the system is still observable. The result is also shown in Table 1. Because the inaccurate parameters are observable, it makes sense to apply an estimator that is adaptive to the system change. In this case the PMU measurement serves two purposes: for the estimation of the state variables and for the real-time update of parameter changes. Once again, UKF is applied to estimate the value of the state variable as well as the parameter variation.

We tested UKF by changing one parameter in Y matrix by 20%. For example, the true value of $\bar{Y}_{12}$ is 80% of Y_{12} given to the UKF. Started from the incorrect model parameters, the UKF uses the PMU measurement with noise to estimate ω_1 and δ_i as well as Y_{12}. The process is able to correct the parameter automatically so that the estimates gradually approach the true value. The result is shown in Fig. 10. Similar tests are carried out for variations

of all other entries in Y. All estimates are convergent with a behavior similar to what shown in Fig. 10.

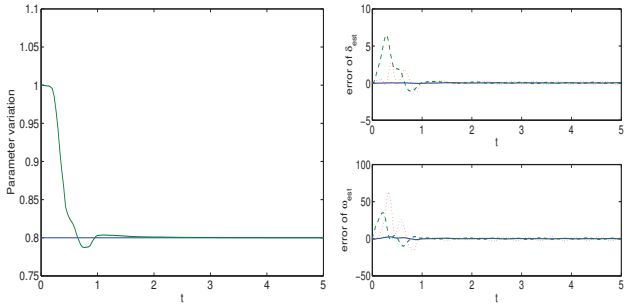

Fig. 10. Adaptive estimation: inaccurate Y_{12}

5. TESTS ON THE 140-BUS NPCC SYSTEM MODEL

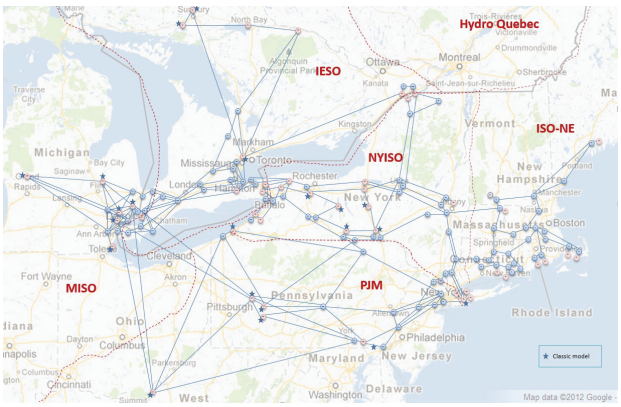

Fig. 11. 140-bus 48-generator NPCC system model

Here, we test the proposed UI and UKF-based state estimation method on the 140-bus 48-generator NPCC system model from Chow [2008] as shown in Fig. 11. The dynamic states of this system is estimated by the square-root unscented Kalman filter (Merwe [2001], Qi [2015]).

5.1 Realistic Generator and Measurement Models

Regarding generator models, 27 of 48 generators are represented in a detailed, widely accepted $4th$-order round-rotor differential equation model in (31) in a d-q reference frame revolving with the rotor and the rest are represented using the $2nd$-order classic model in (10). Thus the number of states is $150 = 4 \times 27 + 2 \times 21$.

$$\begin{aligned}
\dot{\delta}_i &= \omega_i - \omega_R \\
\dot{\omega}_i &= \frac{\omega_R}{2H_i}\left(T_{mi} - T_{ei} - D_i\frac{\omega_i - \omega_R}{\omega_R}\right) \\
\dot{e}'_{qi} &= \frac{1}{T'_{d0i}}\left(E_{fdi} - e'_{qi} - (x_{di} - x'_{di})i_{di}\right) \\
\dot{e}'_{di} &= \frac{1}{T'_{q0i}}\left(-e'_{di} + (x_{qi} - x'_{qi})i_{qi}\right)
\end{aligned} \tag{31}$$

where e'_{qi} and e'_{di} are the transient voltage along q and d axes, i_{qi} and i_{di} are stator currents at q and d axes, E_{fdi} is the internal field voltage, T'_{q0i} and T'_{d0i} are the open-circuit time constants for q and d axes, x_{qi} and x_{di} are the synchronous reactances, and x'_{qi} and x'_{di} are the transient reactances at the q and d axes, respectively.

T_{mi} and E_{fdi} are considered as inputs. For generator i where a PMU is installed, the terminal voltage phaosr $E_{ti} = e_{Ri} + je_{Ii}$ and terminal current phasor $I_{ti} = i_{Ri} + ji_{Ii}$ are measured. See Qi [2015] for the detailed system model about those input, output, and state vectors. Gaussian noise is added to the outputs. The variance for e_{Ri} and e_{Ii} is $(0.05p.u.)^2$ and that for i_{Ri} and i_{Ii} is $(0.05p.u.)^2$.

5.2 Test Results with Accurate Model Parameters

Since the DOA for such a high-dimensional system is difficult to visualize or analyze, we only study its projection onto a subspace about specific directions to disturb the system, i.e. about all "N-1" contingencies each losing a single transmission line following a fault: adding a three-phase short-circuit fault to one end of each line and tripping the line on both ends to clear that fault after a fault clearing time T_c. We do not consider faults that cause instability with a T_c even as short as 0.05s, which is shorter than the response time of most realistic protective relays. Such faults are typically very close to generators and should be avoided all the time. Finally, there are totally 202 contingencies to be considered in the tests.

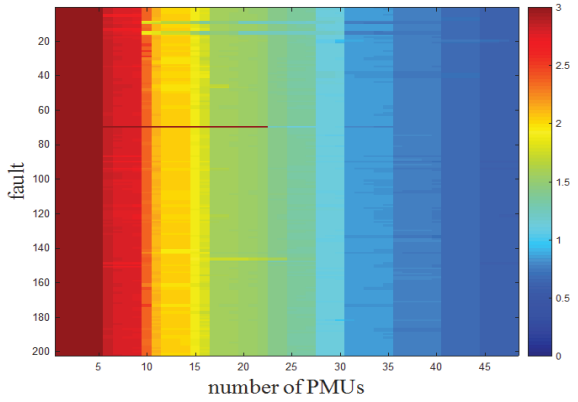

(a) $log(UI)$ with small contingencies ($T_c = CCT/5$)

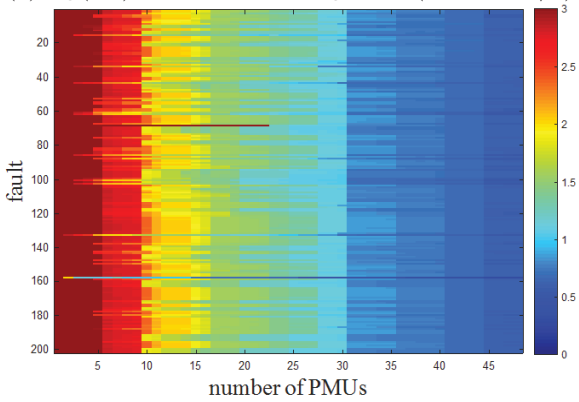

(b) $log(UI)$ with large contingencies ($T_c = CCT$)

Fig. 12. Comparison of the unobservability indices

In order to find the boundary of the DOA following each of those contingencies, we first search for the critical clearing time denoted by CCT, i.e. the maximum T_c without causing instability. To place PMUs in a realistic power grid, we want to demonstrate the necessity of evaluating observability from a nonlinear system perspective, so we evaluate the proposed UI for both small (very stable) and large (marginally stable or unstable) contingencies: we calculate the UI for both $T_c = CCT$ and $T_c = CCT/5$ for each strategy of PMU placement. We consider the

number of PMUs to be placed respectively from 1 to 48 at generator buses. The placement is optimized using the method in Qi [2015].

Fig. 12 visualizes log(UI) for each contingency and for each optimized PMU placement strategy, whose value <1.477, i.e. UI=30 (colored green) corresponds to reasonable observability. From the figure, using 16 PMUs (i.e. 1/3 of generators being measured directly) or more with optimized PMU placement, most UIs are less than 30 (corresponding to green and colder colors) for both small and large contingencies. Compared with plot (b) for small contingencies, plot (a) for large contingencies has some colder colors penetrating into the left warm color regions, and even with PMUs fewer than 16, some contingencies still have UIs $<$ 30. An explanation is that when the system is under large disturbances, especially close to loss of stability, trajectories of state variables may exhibit simpler patterns and might become easier to observe. The estimation results with 16 PMUs for the contingency 26 with UI=22.83 are illustrated in Fig. 13(a)-(b). Fig.14 compares the state estimates with the true values for 5 generators with larger errors, where generators 15, 23 and 24 represented using the $4th$ order model each have state variables δ_i, $f_i = \omega_i/2\pi$, e'_{qi}, and e'_{di}, and generators 34 and 47 represented using the $2nd$ model only have the first two state variables.

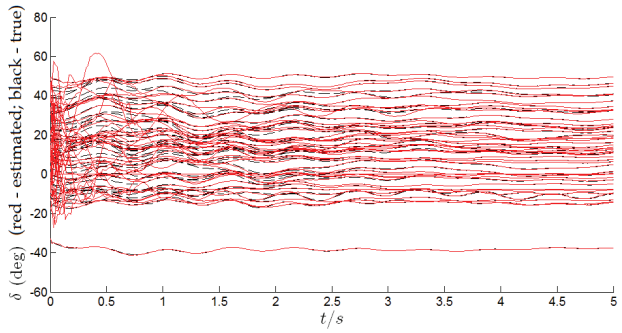

(a) $T_c = CCT/5$

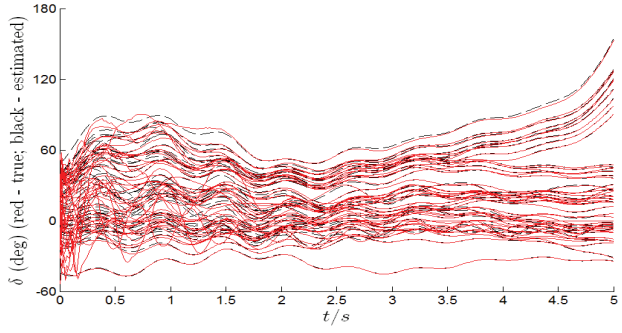

(b) $T_c = CCT$

Fig. 13. Contingency 26: true angles of all generators vs. the estimates by 16 PMUs

5.3 Test Results with Inaccurate Model Parameters

We also test the case with inaccurate model parameters. To quantitatively compare the estimation results, we define the following overall system state estimation error index

$$\epsilon_x = \sqrt{\frac{\sum_{i=1}^{g}\sum_{t=1}^{T_s}(x_{i,t}^{\text{est}} - x_{i,t}^{\text{true}})^2}{g\,T_s}} \tag{32}$$

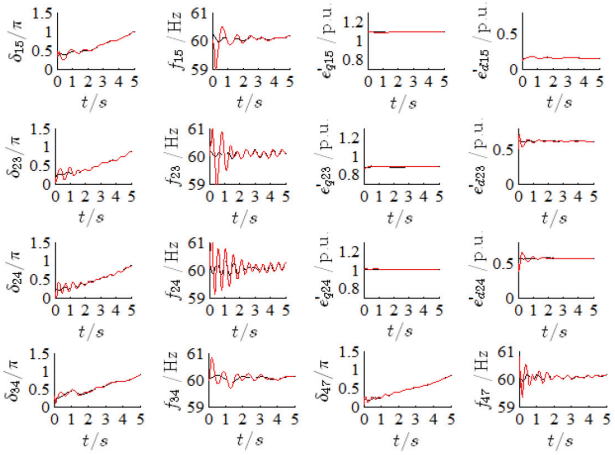

Fig. 14. Contingency 26: true states vs. estimates on 5 generators (15, 23, 24, 34 and 47) with larger errors

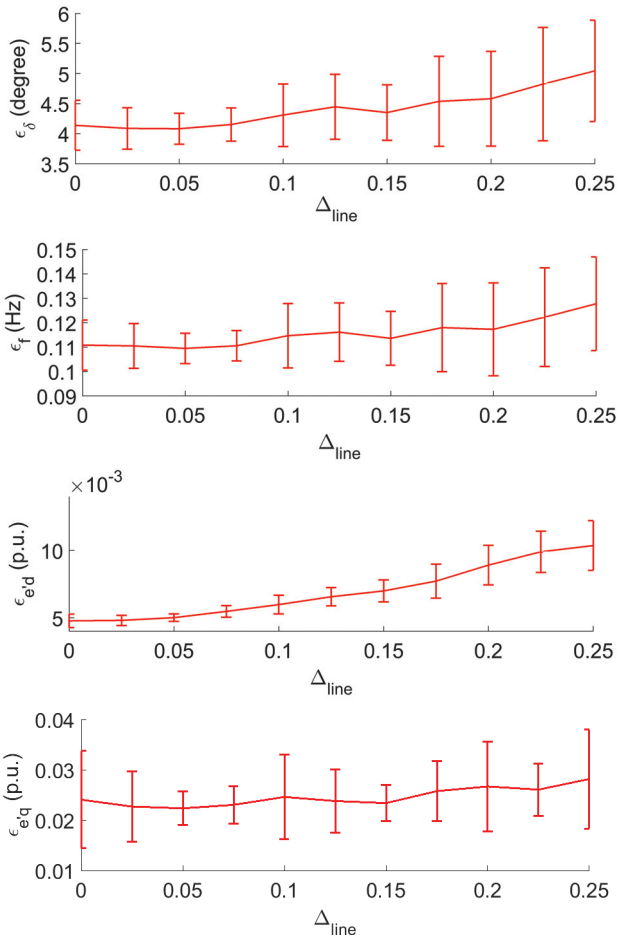

Fig. 15. Contingency 26: State estimation error indexes for random line impedance changes (16 PMUs)

where state variable x_i can be δ_i, $f_i = \omega_i/2\pi$, e'_{qi}, or e'_{di}; $x_{i,t}^{\text{est}}$ is the estimated state and $x_{i,t}^{\text{true}}$ is the corresponding true value for generator i at time step t; T_s is the total number of time steps in the simulation period.

Consider four types of model inaccuracies:

- Type-A: all line impedances have random relative errors uniformly from $[-\Delta_{line}, +\Delta_{line}]$

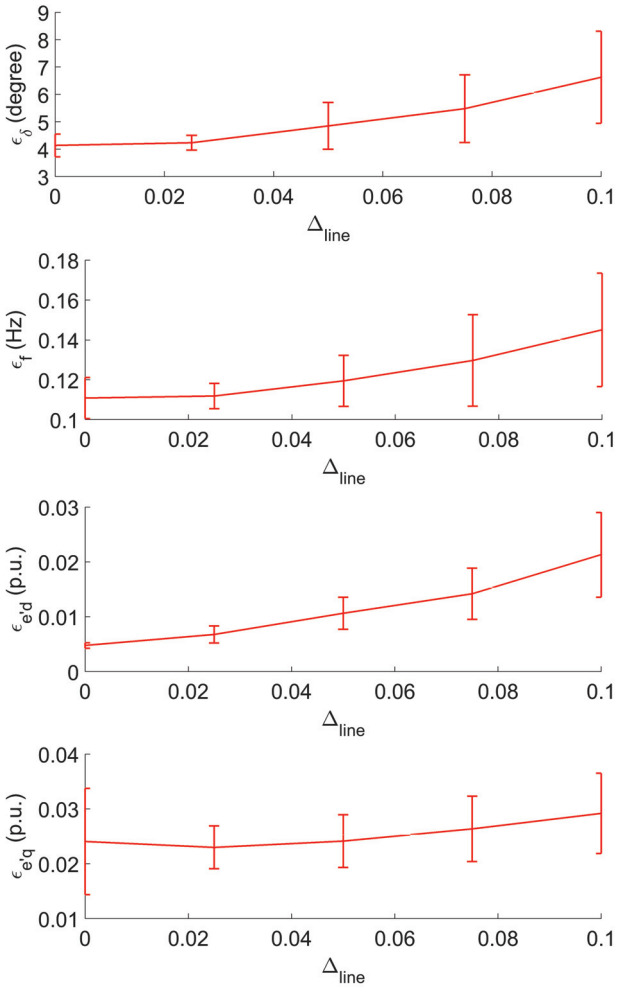

Fig. 16. Contingency 26 (16 PMUs): state estimation error indexes vs. relative load errors

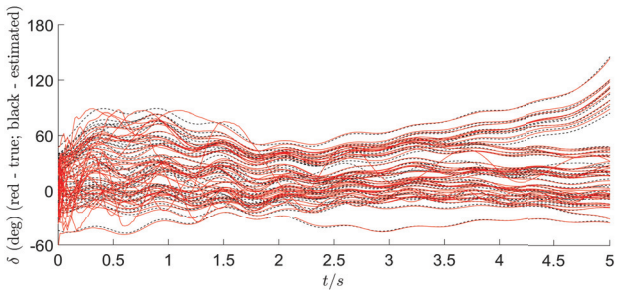

(a) Relative line impedance errors up to 25%

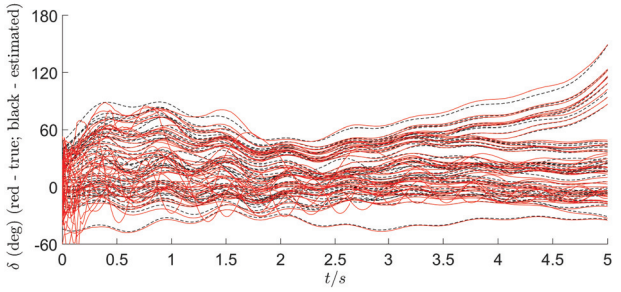

(b) Relative bus load errors up to 10%

Fig. 17. Contingency 26: true angles of all generators vs. the estimates by 16 PMUs with inaccurate parameters

- Type-B: all bus loads have random relative errors uniformly from $[-\Delta_{load}, +\Delta_{load}]$
- Type-C1: the actual system has random one line out of service, which is not told from the model; i.e. an "N-1" condition.
- Type-C2: the actual system has random two lines out of service, which is not told from the model; i.e. an "N-2" condition.

We still test the state estimation using 16 PMUs for the contingency 26 with $T_c = CCT$. Respectively, we generate 50 random cases for each of the four types.

For Type-A and Type-B, it is found that estimation error indexes become significant when $\Delta_{line} = 0.25$ and $\Delta_{load} = 0.1$ (i.e. up to 25% and 10% errors of the true line impedances and bus loads), as shown by Fig. 15 and Fig. 16 on the estimation error indexes with bar charts indicating their standard deviations. Within those thresholds, the angle estimation error is less than 10 degree, which will not significantly impact the judgment of system stability. Fig. 17 illustrates the estimates vs. the true states of two cases respectively from Type-A having $\Delta_{line} = 0.25$ and from Type-B having $\Delta_{load} = 0.1$. The estimates have more oscillations in first 2 seconds but finally correctly track all states. For both cases, 16 PMUs are able to robustly judge stability of the system even with slightly inaccurate parameters.

The histograms about ϵ_δ and ϵ_ω of 50 random cases of Type-C1 and Type-C2 are shown in Fig. 18. 45 out of 50 (90%) Type-C1 cases and 32 out of 50 (64%) Type-C2 cases have $\epsilon_\delta \leq$10 degree and $\epsilon_f \leq 0.2$ Hz. These tests show that, for a majority of unknown outages of one or two lines, state estimates using an inaccurate system model not considering the outage have errors at a low level so as not to influence the judgment of system stability significantly.

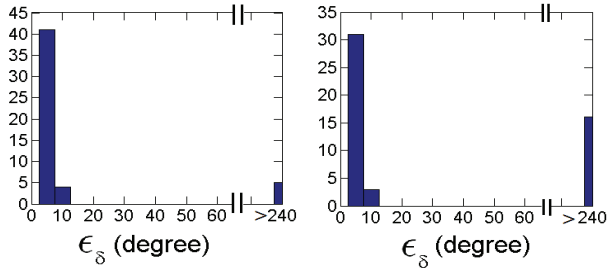

(a) ϵ_δ for Type-C1 (left) and Type-C2 (right)

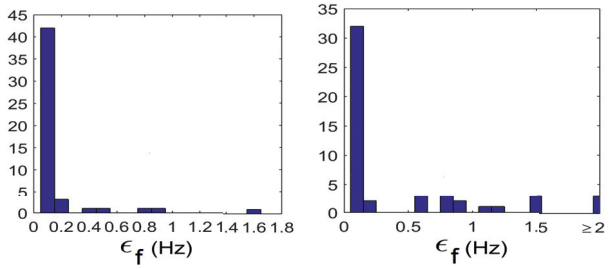

(b) ϵ_f for Type-C1 (left) and Type-C2 (right)

Fig. 18. Contingency 26 (16 PMUs): Histograms on state estimation error indexes

6. CONCLUSION

The concept of observability and its computational algorithms can be used as a tool to evaluate the effectiveness of a PMU network. For a 9-bus model with three generators, a single PMU makes the entire system observable at the boundary of the DOA. Using the data from the PMU, all state variables can be estimated using virtue sensors such

as a UKF. The computation shows that observability is not robust to model uncertainties. However, the unknown parameter variations are observable. It implies that adaptive estimation method should be used to provide reliable state estimates. The proposed methodology has also been tested on a realistic 140-bus 48-generator NPCC system model. The results indicate that 1/3 of generators being measured directly by PMUs with an optimized placement can make the system state reasonably observable for most of "N-1" contingencies especially when the system approaches instability, i.e. $T_c = CCT$. Also, the proposed UKF-based estimation method can track system states for stability monitoring even with some inaccurate model parameters in line impedances, bus loads and the network topology. These features are important for real-time power system stability monitoring and control (Sun [2011a,b, 2012]).

REFERENCES

W. Kang. L. Xu (2009). Computational Analysis of Control Systems Using Dynamic Optimization. *arXiv*: 0906.0215v2.

W. Kang. L. Xu (2009) A Quantitative Measure of Observability and Controllability. *The 48th IEEE CDC*, Shanghai, China.

Arthur J. Krener, K. Ide (2009). Measures of unobservability. *The 48th IEEE CDC*, Shanghai, China.

W. Kang, L. Xu (2012) Optimal placement of mobile sensors for data assimilations. *Tellus A*, 64, 17133.

A. K. Singh, J. Hahn (2005). Determining optimal sensor locations for state and parameter estimation for stable nonlinear systems. *Ind. Eng. Chem. Res.*, 44(15), 56455659.

A. K. Singh, J. Hahn (2006). Sensor location for stable nonlinear dynamic systems: Multiple sensor case. *Ind. Eng. Chem. Res.*, 45(10), 36153623.

T. Baldwin, L. Mili, J. Boisen, M.B. Boisen, R. Adapa (1993) Power system observability with minimal phasor measurement placement. *IEEE Trans. Power Syst.*, 8(2), 707–715.

B. Xu, A. Abur (2004). Observability analysis and measurement placement for systems with PMUs. *in IEEE Power Syst. Conf. Expo.*, Vol. 2, 943–946.

B. Gou (2008). Optimal placement of PMUs by integer linear programming. *IEEE Trans. Power Syst.*, 23(3), 1525–1526.

S. Chakrabarti, E. Kyriakides. (2008). Optimal placement of phasor measurement units for power system observability. *IEEE Trans. Power Syst.*, 23(3), 1433–1440.

B. Milosevic, M. Begovic (2003) Nondominated sorting genetic algorithm for optimal phasor measurement placement. *IEEE Trans. Power Syst.*, 18(1), 69–75.

F. Aminifar, C. Lucas, A. Khodaei, M. Fotuhi-Firuzabad (2009). Optimal placement of phasor measurement units using immunity genetic algorithm. *IEEE Trans. Power Del.*, 24(3), 1014–1020.

Q. Gong, W. Kang, I. M. Ross (2006). A Pseudospectral Method for the Optimal Control of Constrained Feedback Linearizable Systems. *IEEE Trans. Automatic Control*, 51(7), 1115-1129.

S. J. Julier, J. K. Uhlmann (2004). Unscented filtering and nonlinear estimation. *Proceedings of the IEEE,* 92(3), 401-422.

P. M. Anderson, A. A. Fouad (1994). *Power Systems Control and Stability*, IEEE Press.

W. Kang, K. Sun (2013) Detection of Instability Using Synchrophasors: A Theoretical Investigation on Observability with Synchrophasor Networks. *EPRI Technical Report*, No. 3002002061.

W. Kang (2011) The consistency of partial observability for PDEs. *arXiv*: 1111.5846v1.

F. Fahroo, I. M. Ross (1998). Costate Estimation by a Legendre Pseudospectral Method. *The AIAA Guidance, Navigation and Control Conference*, Boston, MA.

J. Qi, K. Sun, W. Kang (2015) Optimal PMU Placement for Power System Dynamic State Estimation by Using Empirical Observability Gramian. *IEEE Trans. Power Systems*, vol. 30, pp. 2041-2054, July 2015.

K. Sun, W. Kang (2014) Observability and Estimation Methods Using Synchrophasor. *The 19th IFAC World Congress*, Cape Town, South Africa.

K. Sun, K. Hur, P. Zhang (2011) A New Unified Scheme for Controlled Power System Separation Using Synchronized Phasor Measurements. *IEEE Trans. Power Systems* 26(3), 1544-1554

K. Sun, S. T. Lee, P. Zhang (2011) An Adaptive Power System Equivalent for Real-time Estimation of Stability Margin using Phase-Plane Trajectories. *IEEE Trans. Power Systems*, 26(2), 915-923

K. Sun, X. Luo, J. Wong (2012) Early Warning of Wide-Area Angular Stability Problems Using Synchrophasors. *IEEE Power & Energy Society General Meeting.* San Diego, CA, USA

J. Chow, G. Rogers (2008) User manual for power system toolbox, version 3.0, 1991–2008.

M. Baechle, V. Knazkins, M. Larsson, P. Korba, (2014) Improved Rotor Angular Speed Measurement: a Key for Proper Power Grid Stabilization. *IEEE Power & Energy Society General Meeting.* National Harbor, MD, USA

Dobson, I., Carreras, B.A., Lynch, V. E., Newman, D.E. (2001) An initial model for complex dynamics in electric power system blackouts. 34th Hawaii Int. Conf. Syst. Sci., 710718.

Qi, J., Dobson, I., Mei, S. (2013) Towards estimating the statistics of simulated cascades of outages with branching processes. IEEE Transactions on Power Systems, 28(3), 3410-3419.

Qi, J., Sun, K., Mei, S. (2015) An interaction model for simulation and mitigation of cascading failures. IEEE Transactions on Power Systems, 30(2), 804-819.

Van Der Merwe, R., Wan, E.A. (2001) The square-root unscented Kalman filter for state and parameter-estimation. IEEE Int. Conf. Acoustics, Speech, and Signal Processing (ICASSP), 6, 34613464.

Qi(2015) Qi, J., Sun, K., Wang, J., Liu, H. (2015) Dynamic state estimation for multi-machine power system by unscented Kalman filter with enhanced numerical stability. arXiv:1509.07394.